**UCRL-ID-125795**

# Ignition and Initiation Phenomena: Cookoff Violence Prediction

J. L. Maienschein and A. L. Nichols III

January 15, 1997

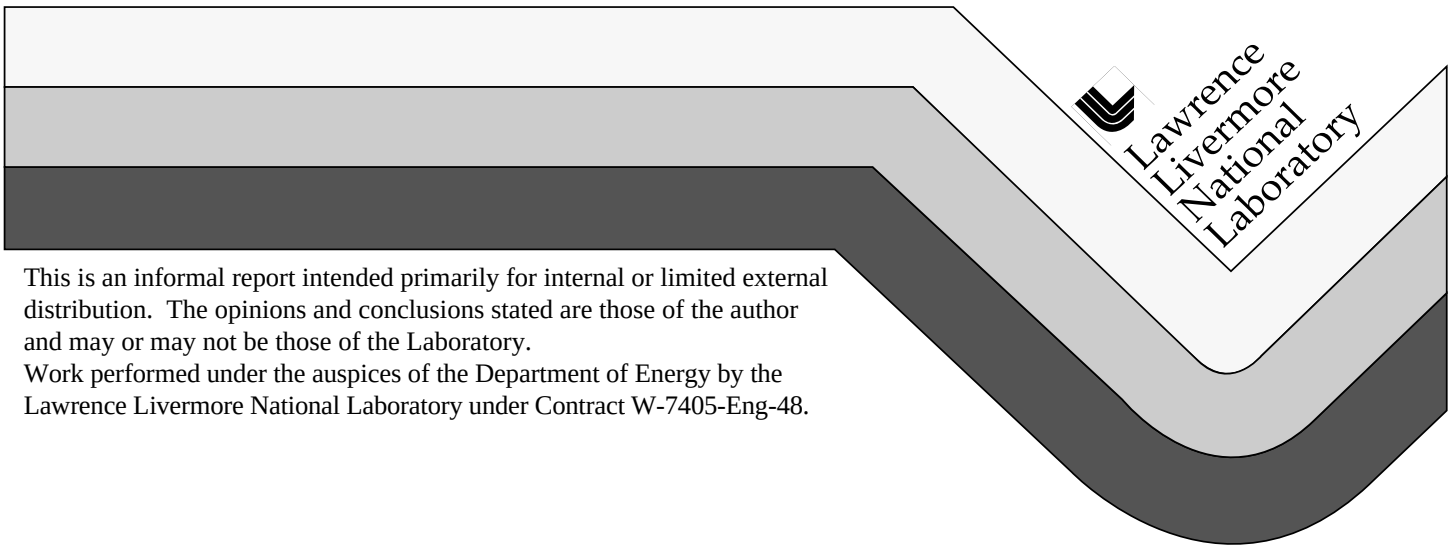



Work performed under the auspices of the Department of Energy by the Lawrence Livermore National Laboratory under Contract W-7405-Eng-48.

# Ignition and Initiation Phenomena: Cookoff Violence Prediction

Jon L. Maienschein
Albert L. Nichols III
Lawrence Livermore National Laboratory
(510) 423-1816
maienschein1@llnl.gov

## Abstract

The Ignition and Initiation Phenomena program is focused on the prediction of the violence of cookoff response for energetic materials and their systems. We are developing analytical tools for this task in the form of the ALE3D computer code, and we are measuring key response parameters for HMX-based energetic materials for application in ALE3D. ALE3D is a fully-coupled thermal/chemical/mechanical hydrocode that can incorporate all such processes during the relatively slow heating of the energetic material and also during the rapid ensuing reaction wherein the degree of violence is determined. We describe the status of and future plans for ALE3D development and show modeling results using ALE3D for the U.S. Navy Variable Confinement Cookoff Test, which has been identified as a test case for development of predictive capability. The key response parameter under study is the burn rate at high pressures and temperatures characteristic of cookoff environments. We report burn rates for LX-04 for pressures of 10–600 MPa and temperatures of 300–453 K and discuss future plans. We also present initial data from a thermocouple embedded in the burning sample to measure thermal diffusivity under burn conditions.

## Introduction

We seek in this program to develop a predictive capability of the violence of thermal events (i.e., slow and fast cookoff) for systems containing energetic materials. This requires that we gain understanding of the fundamental thermal response of energetic materials and that we develop the necessary analytical tools to apply this knowledge to the prediction of violence. Currently we (and others) can predict the time of reaction for a specific time-temperature profile, but reliable prediction of violence is not feasible. To properly assess the hazards from an event involving heating, prediction of the violence of thermal response is necessary. This issue is of interest in the DoD and DOE communities; Dr. Thomas Boggs at NAWC-China Lake and Dr. Ruth Doherty at NSWC-Indian Head have shown particular interest in this work.

The degree of violence of the thermal response of an energetic material is largely controlled by the balance between heat release by exothermic combustion reactions and heat

dissipation by thermal diffusion. In addition, the physical properties of energetic materials under cookoff conditions will strongly affect the violence of reaction. To characterize the fundamental thermal response of energetic materials, we are therefore measuring the burn rate (i.e., rate of heat release) and thermal diffusivity of pristine and thermally-degraded energetic materials at high temperatures and pressures. In our measurements we approach as closely as possible the conditions that exist during cookoff of energetic materials, with pressure of thousands of atmospheres and temperatures of several hundred degrees Celsius. This year we completed measurements on an HMX-Viton formulation (LX-04) from 295 to 435 K; we are currently starting measurements on thermally-degraded LX-04.

We hope to assess the effect of thermal damage on violence by studying burn rates at different levels of thermal decomposition. By coupling our measurements on preheated samples with the kinetic data for HMX thermal decomposition being developed by Dr. Richard Behrens at Sandia National Laboratory and by others, we hope to quantify the link between formation of other compounds by thermal decomposition and the resultant burn rate. Therefore, from this experimental effort, we will have data on the high-pressure burn rate of HMX and of HMX containing thermal decomposition products. We will then develop a burn model for HMX that can be incorporated into our analytical tool, ALE3D.

We must consider very different characteristics (when compared with traditional shock initiation and propagation) to undertake analysis and prediction of violence of cookoff response. First, the time scales associated with the response range from minutes to days to milliseconds to microseconds. Second, the mechanism of energy transfer is by thermal transfer instead of shock propagation. Third, the change in composition is directly a function of the temperature and must be modeled as such, instead of modeling it as either a *fait-accompli* or as a pressure driven reaction. Fourth, the process can be relatively slow so that the energetic material and its containment are subject to deformation in the elastic regime for the major portion of the response, instead of very quickly transitioning to plastic modes. Fifth, because the reactions occur slowly, the composition of the energetic material is a mixture of reactants, intermediates, and final products throughout the duration of the calculation. This is very different from detonation modeling where material is either fully unreacted or fully reacted in all but a small region of space and time. Therefore, it is more important to model the properties of the material mixture because it is no longer the exception but rather the rule.

To incorporate the characteristics, we are transforming ALE3D from a 3-D hydrocode into a 3-D coupled thermal/chemical/mechanical code by adding several new capabilities. These include implicit thermal transport, thermally driven reactions, models for both the thermal and mechanical properties of chemical mixtures, second order species advection, and implicit hydrodynamics. The resultant ALE3D will allow calculation of the complete cookoff problem in one code, including prediction of the violence of the reaction and resulting metal movement.

As part of ALE3D development, we are applying it to problems of interest to DoD and DOE. In particular, the Navy Variable Confinement Cookoff Test (VCCT) offers an extensive database of thermal response under defined conditions. Prediction of cookoff

violence as measured by the VCCT has been identified by Dr. Boggs as a "Grand Challenge" problem for the thermal response community, and our modeling efforts are aimed at that challenge. Once developed, our analytical tools will allow us to relate small-scale experimental data to large-scale thermal response predictions without extensive large-scale experiments.

We note that physical properties of heated and degraded energetic materials must also be characterized in order to allow accurate prediction of violence. This is beyond the scope of this program, but is being addressed in other work at LLNL, Sandia National Laboratories, and elsewhere.

## Experimental Work: Burn Rates and Thermal Diffusivity of HMX–Viton Formulations

### Burn Rate Apparatus

Our hybrid strand burner-closed bomb system, shown in Figure 1, combines the features of a traditional closed-bomb burner with those of a traditional strand burner. In a standard closed-bomb burner, pressure in the combustion chamber is the only measurement, with no measure of the surface regression rate to check combustion uniformity; the data from samples that burn erratically are particularly hard to interpret. The standard strand burner provides direct measurement of the surface regression rate in a large volume at constant pressure, giving only one data point of rate vs pressure in each experiment; further, the large volume required for isobaric operation means that operation at high pressures is generally not practical. In contrast, our hybrid strand burner-closed bomb system burns a sample in a small constant-volume, high-pressure chamber; temporal pressure data and burn front time-of-arrival data provide surface regression and mass regression data for a range of pressures in one experiment. We use a load cell to measure the temporal pressure in the bomb, and detect the arrival of the burn front by the burning through of wires embedded in the sample. A high speed digitizer captures the data for subsequent analysis. This year we also designed and acquired components to add a pressure transducer to the system for direct measurement of pressure within the burner.

The sample in the hybrid system, shown in Figure 2, is a cylinder 64 mm long and 6.4 mm in diameter, made of five to seven pellets stacked on end; silver wires (75 μm in diameter) are inserted between each pair of pellets along the sample. The burn front time-of-arrival data are provided by monitoring the time at which these wires are burned through after ignition at the top of the sample. After assembly, the entire sample is coated with epoxy (Epon 828 with Versamid 140 catalyst) to prevent burning of the sample surface. This limits the burn front to the face of the sample, resulting in a laminar burn.

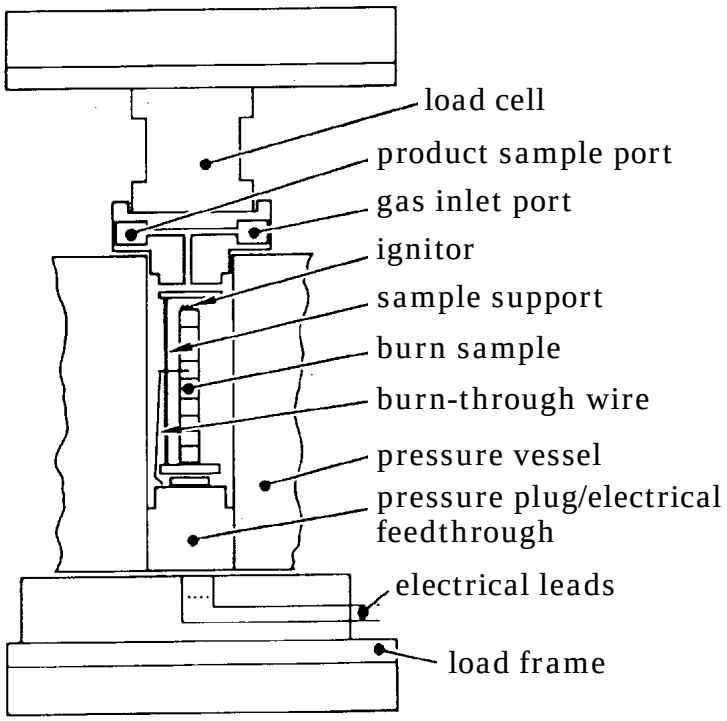


**Figure 1. Schematic of hybrid strand burner. Pressure vessel can be pressurized up to 400 MPa prior to burn; final pressures may exceed 1 GPa. A sample, 64 mm long and 6.4 mm in diameter, is ignited at the top by a hot wire imbedded in boron potassium nitrate. Burn is monitored by sequential breaking of burn-through wires as flame progresses down the sample, as well as by temporal pressure signal.**

The burn rate is calculated from the elapsed time between wires breaking on each end of each pellet. We embed a rapid-response, 5-μm-thick foil thermocouple between two of the pellets, and record the temporal thermal profile as the burn front approaches that location. From the thermal profile, we calculate the thermal diffusivity at the actual conditions in the burning material. We incorporate a heater and thermocouple into the sample holder to allow measurements with preheated samples. More details on the hybrid strand burner-closed bomb system are given by Tao[1,2] and by Maienschein. [3,4]

During this reporting period, we made several upgrades to the system. We improved the electronics and replaced copper burn wires with silver wires to allow more reliable burn wire data acquisition. We added a groove to one face of each pellet to eliminate the gap caused by the presence of the burn wire. We replaced the original HMX/FEFO ignition material with HNS, to allow operation at high temperatures. We also improved the high-temperature capability, testing the equipment up to 520 K. Another development was refining the methods to build the burn tower assemblies to gain efficiencies in their manufacture. By applying all these upgrades, we were able to achieve a steady running rate of more than one run per day for a period of several weeks, significantly faster than was possible in the past.

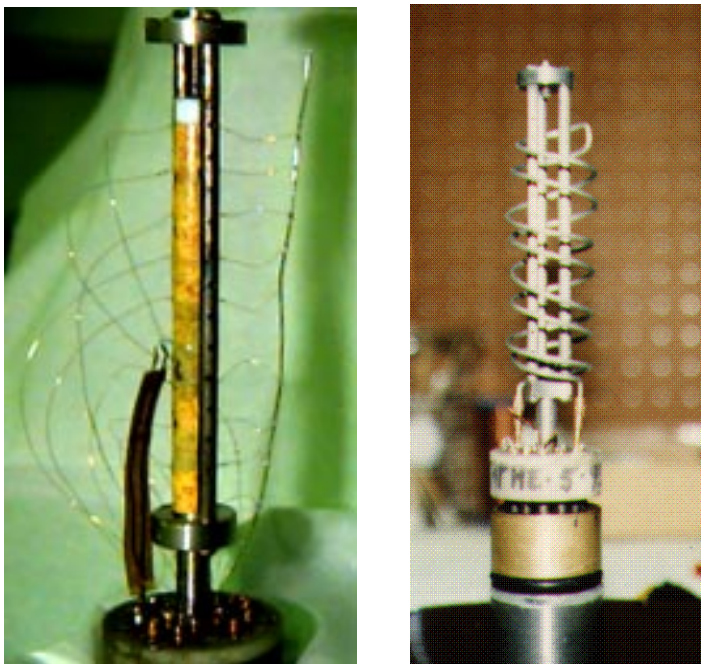

**Figure 2. Sample holder and sample for hybrid strand burner. Photo on left shows a sample, 64 mm long and 6.4 mm in diameter, in a holder. Wires placed between each pellet—to indicate arrival of the burn front—are visible. The thermocouple projecting up from the base is embedded between two pellets to measure the temporal thermal profile in the sample. Photo on right shows nichrome heating element used in preheated measurements.**

## Experimental Plan

We would ideally measure the burn rate of pure HMX at high temperature and pressure. However, it is not practical to make pellets of pure HMX that will burn uniformly. To get uniform planar burn down the length of the sample, the sample must contain small-particle HMX in a low-porosity pellet. The presence of large, easily fractured HMX particles in burn samples leads to irregular deconsolidative burning, with the flame front propagating rapidly through fractures that form at the flame front.[1,2] The presence of voids in the sample also leads to irregular burning as the flames propagate through the voids. Unfortunately, pure small-particle HMX cannot be pressed into high-density, void-free pellets.

We have chosen instead to measure the burn rate of HMX with Viton A binder. Three standard LLNL formulations, LX-07, LX-04, and LX-11, contain small-particle HMX (so-called LX-04 grade) with 20 wt%, 15 wt%, and 10 wt% Viton A, respectively. It is not possible to go below 10% binder with the small-particle HMX because the high surface area of the small particles requires at least 10% binder to give a practical formulation. Most of our measurements are with LX-04, but we also test LX-07 and LX-11 to check the effect of binder concentration on burn rate. If we see significant effects, we can extrapolate to zero binder to estimate the burn rate of pure HMX. Our pressed pellets have densities ranging from 98.0 – 99.3% of theoretical maximum density.

Last year we reported burn rate measurements at initial temperatures between 293 K and 423 K, with initial pressure of 200 MPa. Our results at elevated temperatures were not reliable. The burn wires did not report reliably when hot, and we had to resort to calculation of calibration factors to relate pressure to mass burned in order to calculate a burn rate.[3] We also had not measured burn rates at lower pressures. This year we completed a set of burn rate measurements for LX-04 with initial temperatures of 293 K and 435 K, with direct measurement of the burn rate from burn wire data. By going to 435 K, we heated the samples above the β–δ phase transition in HMX of ≈ 430 K to study the effect of that transition on burn rate. We also extended the pressure range down to 10 MPa to allow comparison of our results with literature data for HMX. The results of this year's efforts represent a complete set of data on LX-04 burn rates; these will be published in the literature.

## Experimental Results

### Burn Rate of LX-04 at Ambient Initial Temperature

Our results with LX-04 at ambient initial temperature are shown in Figure 3. The data taken this year are consistent with those from earlier periods but show much less scatter. In addition, we have extended the pressure range to both higher and lower pressures. The low-pressure data are shown with expanded scale in Figure 4. Again the data show reasonable scatter. The linear fit to all the burn rate data, shown in Figure 3, is reproduced in Figure 4; it represents a good fit to the low pressure data. To use a power-law rate law, we plot the burn rate data in log-log coordinates; as shown in Figure 5, this results in a excellent description of the data.

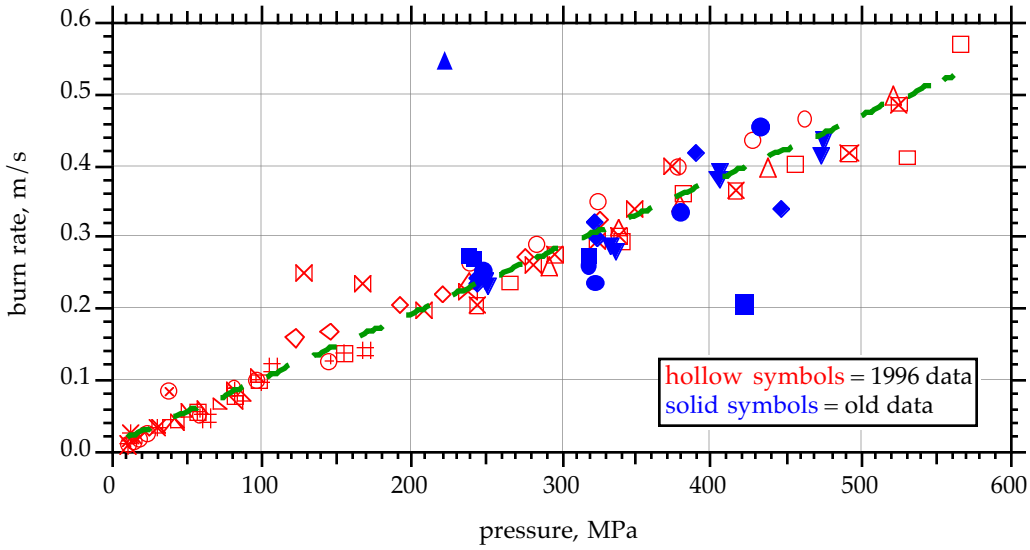


**Figure 3. Burn rate data for LX-04 at ambient initial temperature for pressures of 10 to 580 MPa. Solid symbols show data taken in previous years, hollow symbols show data during this reporting period. Each symbol represents the rate measured by the time difference between two adjacent wires. All measurements from a given run are shown by the same symbol. The dashed line shows a linear fit to the data: burn rate = 0.0077 + 0.000918 P, with $r^2 = 0.98$.**

In Figure 3 we see two anomalously high points at 128 and 168 MPa. When we inspect the pressure data for that run, shown in Figure 6, it is clear that these points do represent an unusually rapid burn and not erroneous measurements. We have not been able to identify a cause for this behavior, and tentatively conclude that these fast-burning segments were different from the others in some way. Despite the care taken to make all samples identical, there is apparently enough sample-to-sample variation to cause the observed fast burn rate. We surmise that much of the scatter in the data shown in Figure 3 is due to sample-to-sample variation of a lesser degree, with run 96025 representing an extreme case.

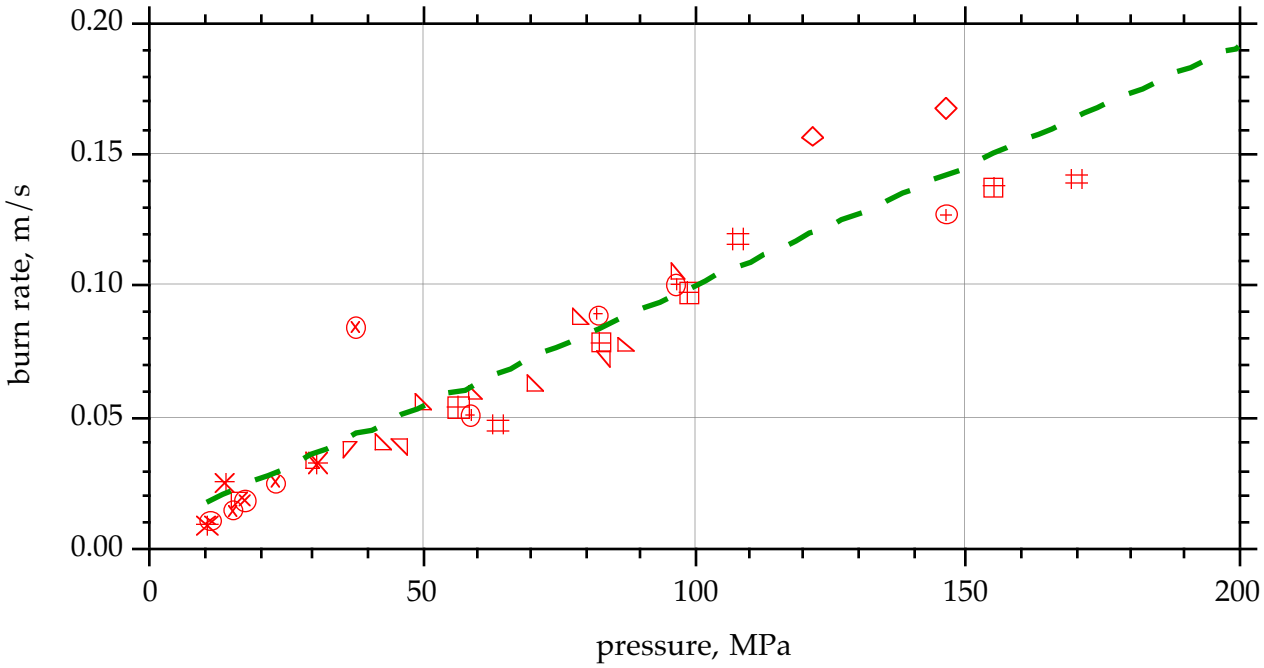


**Figure 4. Burn rate data for LX-04 at ambient initial temperature for pressures of 10 to 170 MPa. Each symbol represents the rate measured by the time difference between two adjacent wires. All measurements from a given run are shown by the same symbol. The dashed line shows the linear fit from Figure 3, calculated from all burn rate data.**

We compare our measured burn rates for LX-04 with burn rates for HMX in Figure 7. The data of Boggs[5] and of Derr[6] are for pure HMX in both pressed pellet and in crystal forms. We see that the burn rates are similar for the pure HMX and for LX-04, with the rate for LX-04 being slightly slower due to the presence of 15% Viton binder. The close correspondence of our measured data to the literature values supports the validity of our measurements.

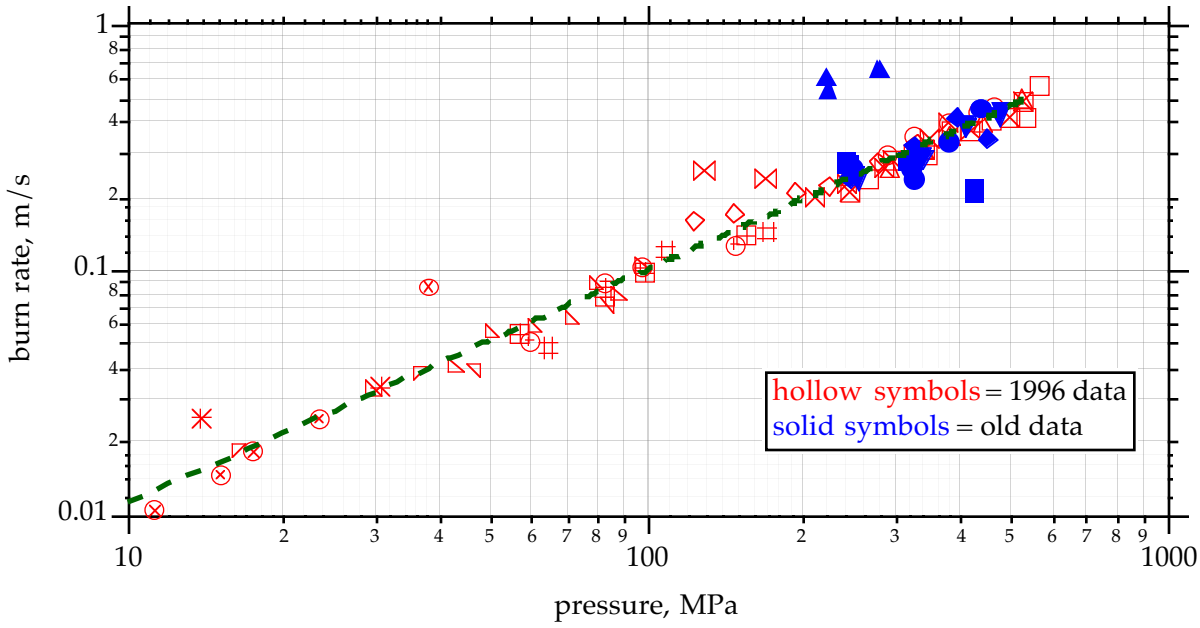


**Figure 5. Burn rate data for LX-04 at ambient initial temperature for pressures of 10 to 580 MPa, plotted for power-law fit. Dashed line is linear fit in log-log coordinates: burn rate = 0.00124 P $^{0.954}$.**

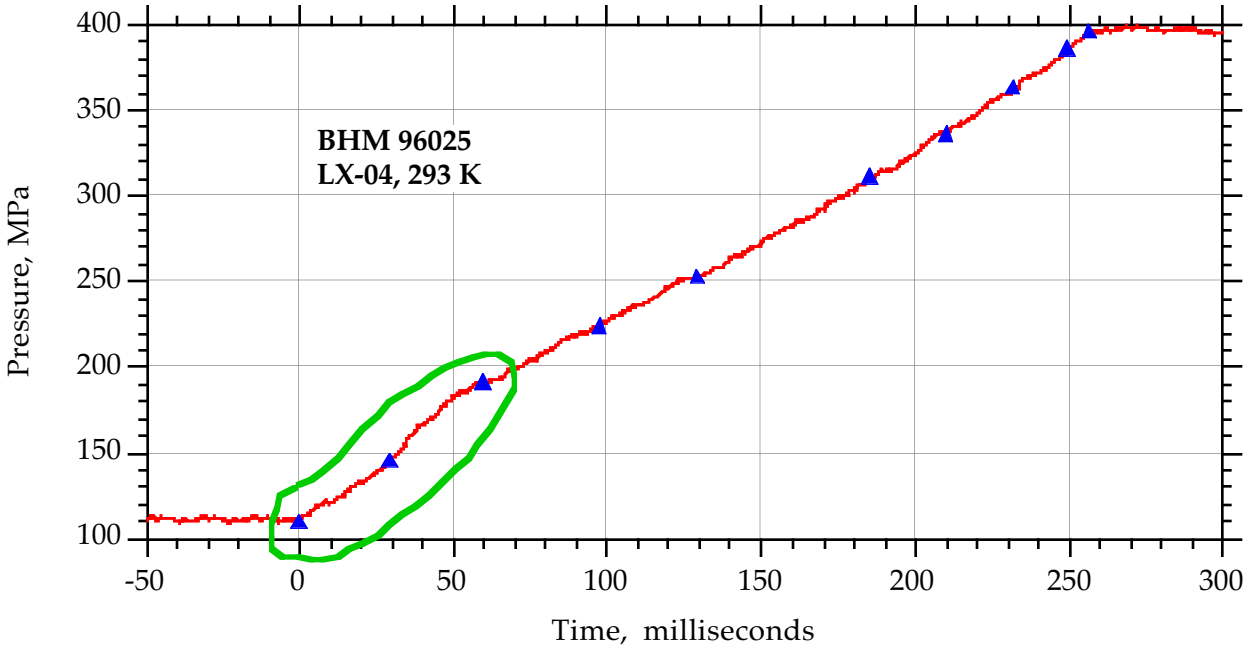


**Figure 6. Pressure-time data for run BHM 96025. The triangle symbols indicate the wire reporting times, with ordinate values arbitrarily matched to the pressure data. The slope of the pressure-time data in the circled region is higher than the slope of the later data, indicating high burn rates in these segments. The burn rates from the corresponding wires are the anomalously high points at 128 and 168 MPa in Figure 3.**

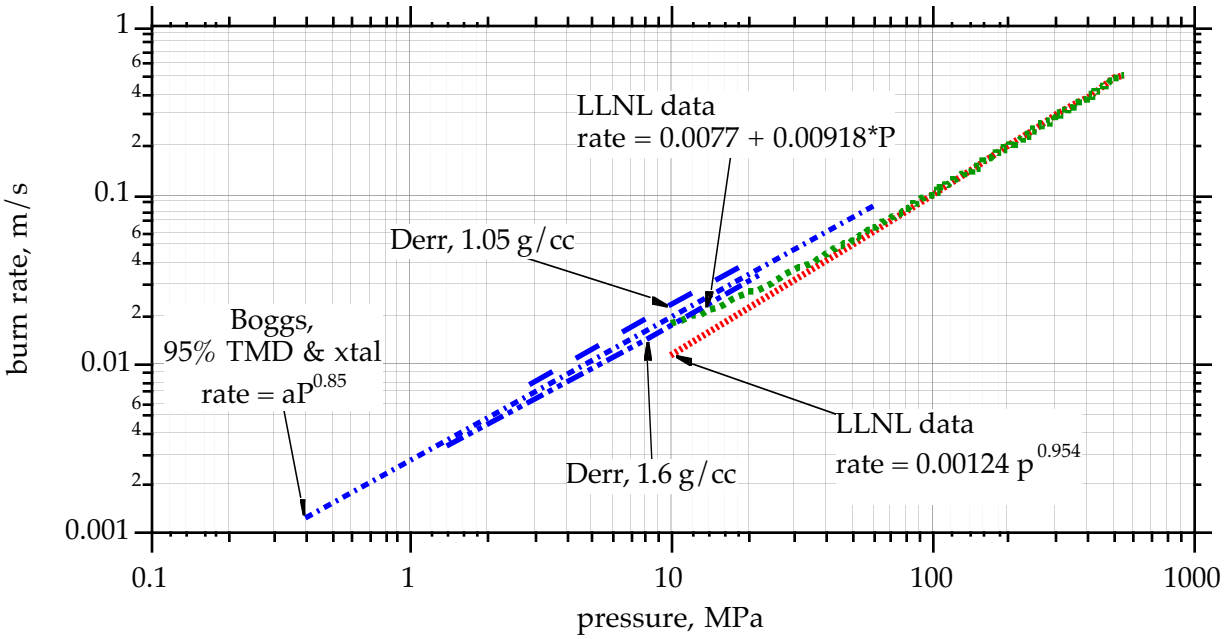


**Figure 7. Comparison of measured burn rates of LX-04 and literature data for HMX burn rates of Boggs[5] and of Derr.[6]**

## Burn Rate of LX-04 at Elevated Initial Temperature

We conducted several runs with LX-04 preheated to 423 K and 453 K, the latter chosen such that the material is heated past the β–δ phase transition. In these experiments the samples were heated to the final temperature and held there for about 10 minutes before burning. Based on Behrens' thermal decomposition data for HMX,[7–9] we expect there to be insignificant thermal degradation of the HMX during this heating period; we therefore measure only the effect of increased temperature on the burn rate. The results are shown in Figure 8, where all data points represent burn rates determined by wire reporting times. In work reported last year we calculated burn rates for heated samples from pressure-time data and calibration factors, which is not as accurate because of assumptions that must be made in the calibration process. The data in Figure 8 therefore represent a significant improvement in the accuracy and reliability of burn rate measurements at high temperatures. If we compare the data in Figure 8 with those reported last year as measured from pressure-time data, the burn rates are about the same, but the data reported last year show a higher pressure dependence than we see in the accurate data.

In these first accurate measurements, we see very little effect of temperature on burn rate. In general the burn rate at higher temperatures looks very similar to that at ambient temperature, but perhaps slightly faster. This offers insight into the combustion process, indicating that the rate controlling step of the combustion process is apparently not thermally activated. We also see large scatter in the measurements, particularly when compared to the scatter in Figure 3. We attribute the increased scatter to the variability of samples caused by heating. Thermal expansion of pressed materials can cause differential grain movement, resulting in opening up of channels or voids. These will provide a path for flames to

propagate at a faster rate than in the solid, thereby giving a faster burn rate as observed. We expect that thermal degradation of the HMX will cause further variability, and will explore the effect of thermal degradation in future work, in which we hold the samples at elevated temperature for prolonged periods before burning.

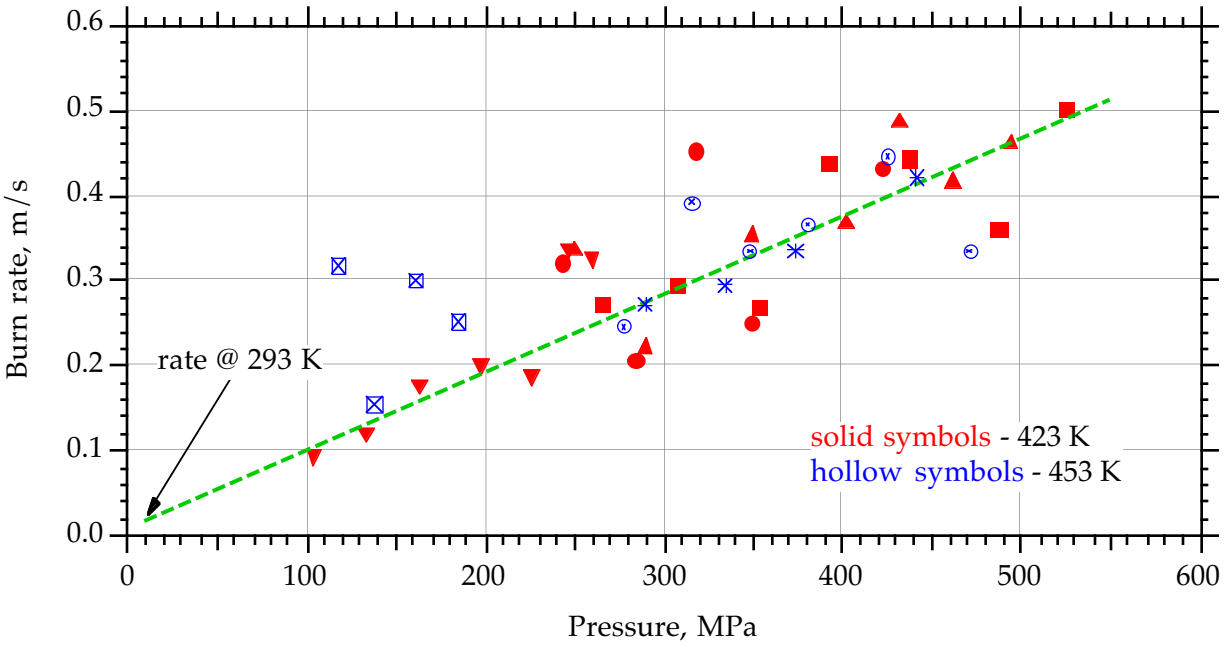


**Figure 8. Burn rate data for LX-04 preheated to 423 K and 453 K. Dashed line is the linear fit to ambient initial temperature burn rate data shown in Figure 3. Samples preheated to 453 K are above the β – δ phase transition.**

## Measurement of Thermal Diffusivity with Embedded Thermocouple

The rapid-response foil thermocouple embedded in the sample is used to measure the temporal profile as the burn front approaches. Sample thermocouple data from an experiment with LX-17 (92.5% TATB, 7.5% Kel-F) is shown in Figure 9a as an illustration of the utility of this technique. We see the temperature smoothly rise from the baseline over a few milliseconds, eventually reaching a maximum. The maximum temperature value is set by the digitizer range and does not represent a maximum temperature during the burn. The thermal diffusivity of the sample is derived from a semilog fit of the temperature rise vs time for the portion of the record that is controlled by thermal diffusion in the sample—i.e., the early and mid-time—and is calculated using the equation:

$$\ln(T - T_0) = A + BR^2/\alpha \qquad (1)$$

where $T_0$ is the initial temperature, A and B are constants, and R is the linear burn rate. The thermal diffusivity, $\alpha$, is defined as:

$$\alpha = \lambda / \rho C_p \qquad (2)$$

where $\lambda$ is the thermal conductivity, $\rho$ the density, and $C_p$ the specific heat. This fit and the associated thermal diffusivity for LX-17 are shown in Figure 9b. This thermal diffusivity value is consistent with a handbook value for the thermal conductivity of 0.8 W/m•K for LX-17.

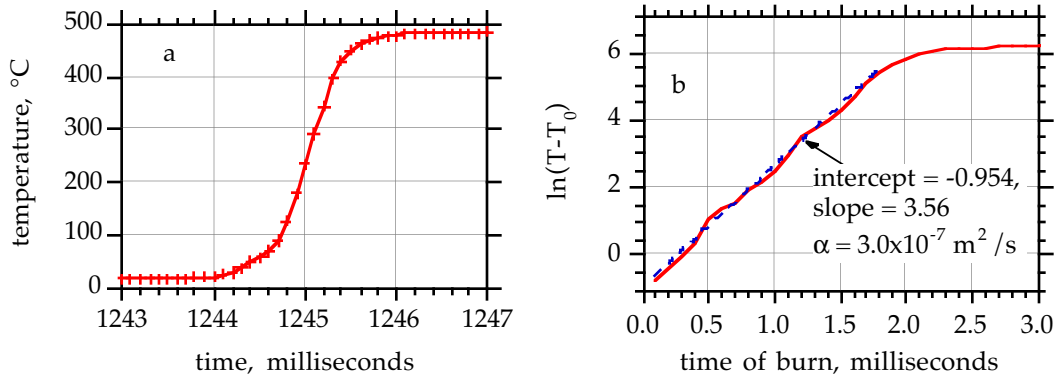


**Figure 9. In-situ thermocouple data from LX-17 burn-rate measurement. Figure 9a shows temperature rise as the burn front approaches the thermocouple location. The maximum recorded temperature is limited by the recording system. The data are plotted in the form of Eq.(1) in Figure 9b.**

Our results with LX-04 were not as good as those with LX-17. The burn rate of LX-04 is much faster, which results in a faster temporal temperature rise. We collected the thermocouple data with LX-04 at a slower-than-desired acquisition rate, resulting in the low-resolution data shown in Figure 10. These data are not sufficient to calculate meaningful thermal diffusivity values, so we will pursue improving this data with LX-04 this coming year. We have, however, demonstrated the utility of this technique for measuring temporal profiles in burning LX-04 energetic material samples.

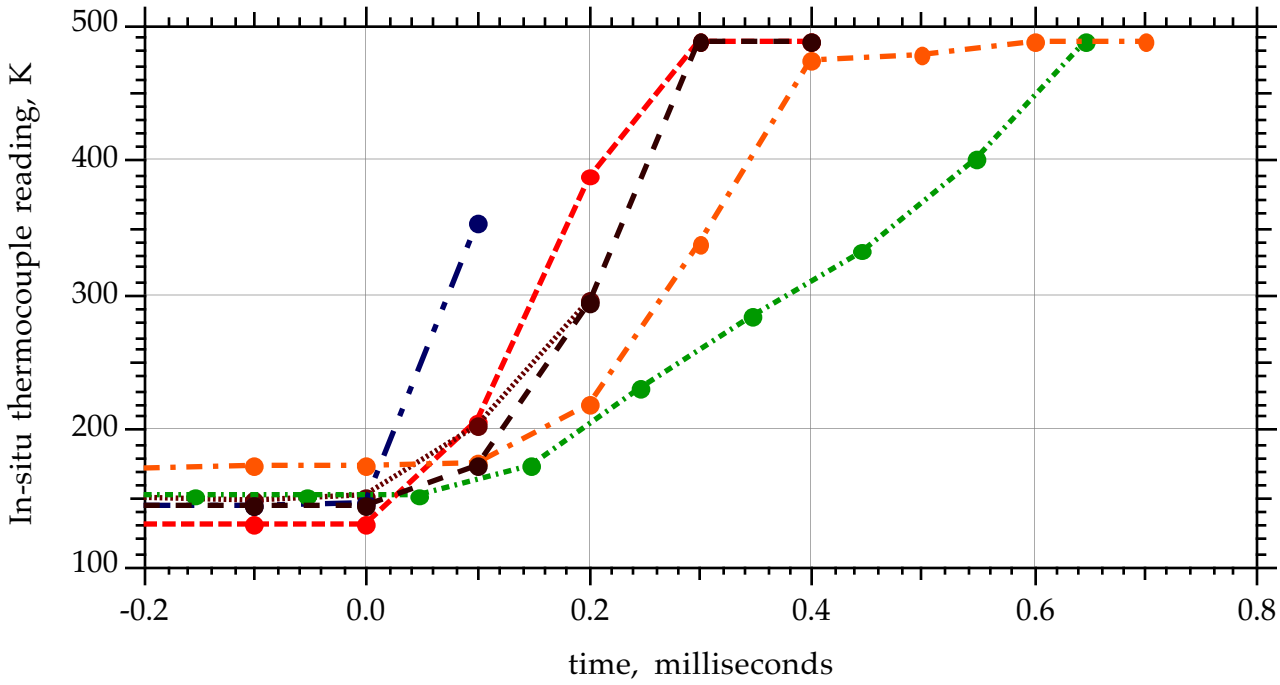


**Figure 10. In-situ thermocouple data for several experiments with LX-04. The time resolution is not satisfactory as a result of the rapid burn rate of LX-04 when compared with LX-17, and we do not calculate thermal diffusivities from this. This method does, however, illustrate the capability to perform these measurements.**

## Summary of Experimental Work and Plans for Next Year

During this year we established a capability for measurement of burn rates over a wide pressure range (10–1000 MPa) and wide temperature range (300–450 K). We have heated the apparatus higher still, to 520 K, and expect to be able to make measurements up to this temperature with suitable energetic materials. We upgraded the equipment and procedures to improve our reliability and increase the rate at which we can perform measurements. We demonstrated the use of an embedded thermocouple to measure thermal diffusivity under actual burn conditions. We also established burn rates for LX-04 across the entire pressure range and at temperatures ranging from 300 to 453 K, with the interesting observation that the burn rate is insensitive to the starting temperature.

In the coming year we plan to extend the HMX studies to samples that are degraded by a prolonged thermal soak in order to determine the effect of HMX degradation on the burn behavior. We also plan to improve the resolution of data from the embedded thermocouple. Following this, other aspects of HMX combustion remain to be studied, including the burn rate of different solid phases; the effect of pressure and confinement during thermal soak and degradation; the effect of lower density LX-04; the effect of higher temperatures; and the effect of another binder. We will also consider separating the effects of thermal expansion and thermal degradation by thermally degrading LX-04 powder and then pressing it into full-density pellets for measurements at room temperature.

# ALE3D Development and Analysis of the U.S. Navy Variable Confinement Cookoff Test

## Description of ALE3D

As discussed in the introduction and in several reports,[3,11,12] we are developing ALE3D as a fully-coupled thermal/chemical/mechanical hydrocode to allow prediction of the violence of thermal events. It offers arbitrary Lagrangian-Eulerian treatment of problems for optimum analysis and includes fully coupled thermal transport and generalized, fully coupled chemical reactions. We have incorporated into ALE3D the capability for implicit and explicit timestepping, with automatic switching from one to the other. This allows calculation of very slow thermal events and very fast hydrodynamic events, just as occur in a cookoff, in one code. Cookoff response inherently involves chemical reaction kinetics, thermal transport, and mechanical response. During heating, a typical energetic material will expand (perhaps with increasing porosity), lose physical strength, and begin to undergo chemical decomposition. In addition, the external container is also being heated, with loss of physical strength. ALE3D offers the ability to integrate all of these aspects because each aspect may control the overall reaction rate under different conditions. ALE3D therefore offers the potential to treat the entire cookoff problem, including hydrodynamic violence of the reaction, in one calculation.

## Improvements to ALE3D

To apply ALE3D to thermal response problems, we have extended its capabilities. For example, when considering response of a material to heat, we must include heat flow, chemical reactions driven by heat, the formation of mixtures from the chemical reactions, the resultant properties of the mixtures (thermal, mechanical, and equation of state), and the overall mechanical response. These mechanisms are included in ALE3D. Thermal mechanisms include thermal diffusion, phase change, thermal contact resistance, and boundary conditions defined in terms of flux, temperature, thermal radiation, and convection. In addition, a proportional, integral, derivative (PID) controller is modeled in ALE3D for the evaluation of experimental data taken with such a controller. Also, a bounded temperature boundary condition may be used in which the boundary temperature sets the minimum temperature at that point; however, exothermic reactions can drive the temperature higher than that boundary condition. Mechanical mechanisms include volumetric adiabatic expansion, elastic-plastic work heating, sliding friction, gravity, and boundary conditions defined by velocity, pressure, or rigid surfaces. Unlimited chemical reactions may be included, and detonation may be modeled as a chemical or mechanical occurrence.

We have made many other improvements to ALE3D, including the treatment of virtual slide surface elements, zonal heat generation for elements containing mixtures, thermal subcycling to improve temperature convergence, and species advection within elements and during implicit calculations. In addition, we have implemented reversible and irreversible stress-strain work heating and an analytic mixture model to include solid thermal expansion. Currently, mixtures of gases and solids are modeled using a simple gamma-law gas formalism and an elastic solid with thermal expansion, allowing analytical solution of the mixture equations.

We have refined the capability of ALE3D to handle calculations with both implicit and explicit time-stepping. The implicit time-step allows use of long time-steps during portions of the calculation when little motion is occurring (e.g., most of the heatup during a cookoff). The size of the implicit time-step is dynamically controlled by ALE3D to achieve the longest time-stepping consistent with accurate solution. When rapid reactions (e.g., deflagration or detonation) begin, ALE3D automatically switches to explicit time-stepping, which is required to properly handle these high-rate events. Last year we reported our initial efforts with implicit/explicit time-stepping. We have refined the technique during this year and show a calculation in the next section where the time-step varies from $10^{4}$ to $10^{-7}$ seconds during the calculation.

More details on the current status of ALE3D are given by Nichols.[12]

## Modeling the U.S. Navy Variable Confinement Cookoff Test

The U.S. Navy Variable Confinement Cookoff Test is a test which has been developed by the Naval Surface Warfare Center as an explosive screening test. The configuration is shown in Figure 11. The test fixture consists of two steel end-plates and a variable thickness steel tube. Inside the steel tube is an aluminum tube which helps distribute the heat uniformly within the device. A cylinder of energetic material is placed between two sets of steel washers. The purpose of the washers is to place the explosive within the uniform heating region. The washers have a hole in the middle which also provides some space for thermal expansion. After an initial heatup, the heaters are used to heat the exterior of the system at a rate of 3.3 °C/hour. The experiment continues until the confinement bursts. An experimental sequence will vary the thickness of the exterior sleeve and characterize the violence of the response as a function of confinement. More details are available from Gibson.[13]

The VCCT is modeled using radiative and convective boundary conditions at all exterior surfaces. The bolts are radiatively connected to the heaters. The heater is treated as a lower bound temperature condition, rising at 3.3 C/hour from 298 K. The HMX-based energetic material reaction is modeled using Tarver's 3-step, 4-species chemical reaction scheme,[14] in which the first two species are treated as solids and the last two as a dense gas and light gas, respectively. The space within the washer is treated as a void material. Typical results are shown in Figure 12. The initial heatup is fairly uniform. After 43 hours the energetic material extrudes into the void spaces at top and bottom. This is a result of the combination of three effects. First, the energetic material is decomposing and has produced a small amount of gas. Second, the energetic material solid species are thermally expanding. Third, the onset of expansion is held off during the early portion of the experiment because of the material strength of the solid species. However, as more gas is produced, the strength drops, letting the material flow. Once expansion has occurred, the system heats uniformly for eight more hours before the onset of violent reaction, during which the end caps bow, the bolts twist, and the outer case expands. During this calculation, the time-step varied from $10^{4}$ to $10^{-7}$ seconds. The implicit/explicit calculation accurately predicts the temperature at which the VCCT reacted to within experimental error and qualitatively reproduces the mechanical response seen. We currently do not have models that will predict the extent of metal fracture

or pressure of gaseous products that would be needed to more quantitatively compare our results to experiment.

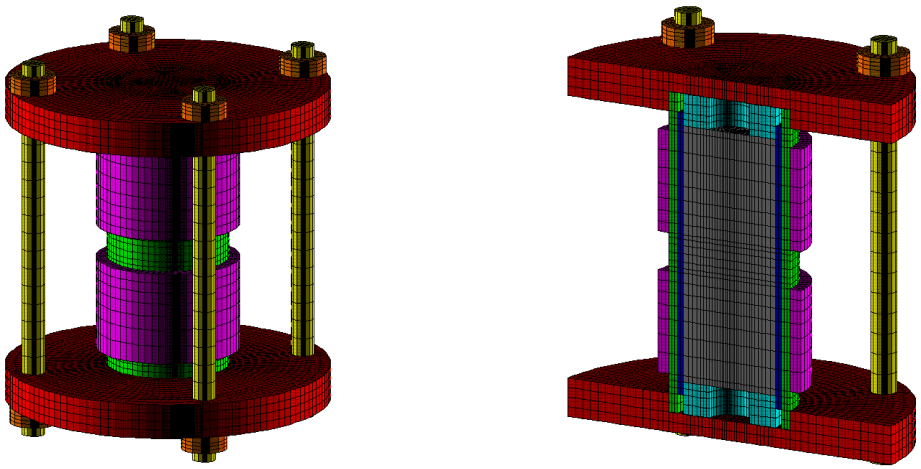

**Figure 11. U.S. Navy Variable Confinement Cookoff Test configuration. Heaters, end plates, confining bolts, and outer steel sleeve are seen in the left-hand view. The cut-away view shows the cylinder of energetic material, with spacers at the top and bottom and with void spaces at the center. Our model incorporates kinetic parameters and physical properties for HMX-based explosives.**

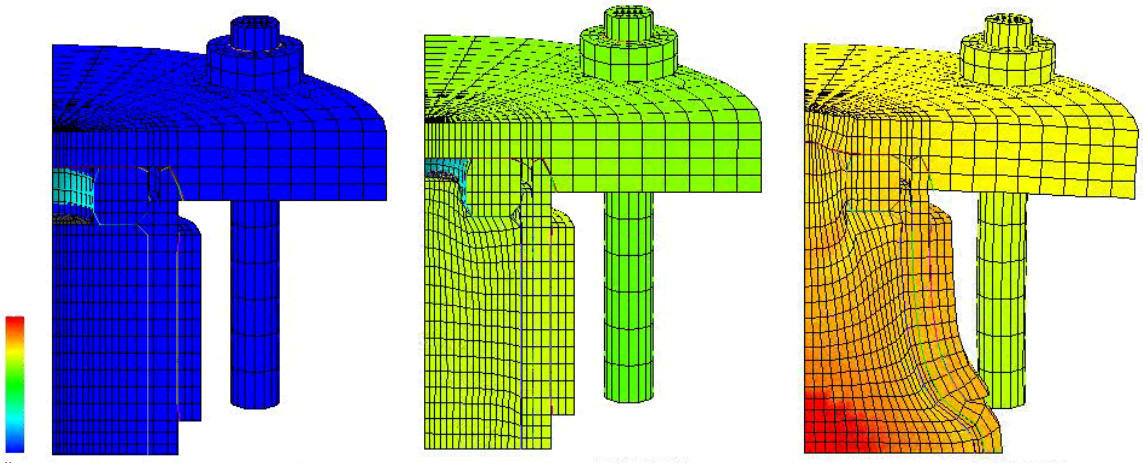

**Figure 12. Typical implicit/explicit results for the VCCT calculation. The color bar (far left) shows temperatures ranging from 300 – 500 K .The left-hand image shows the setup at initial ambient temperature. In the middle image, the explosive is extruding into the void space. This occurs at about 43 hours. At about 53 hours the violent reaction begins, as shown in the right-hand image. The reaction starts at the center, as expected, and deforms the cylindrical confinement, the end cap, and the bolt.**

The VCCT calculation shows the importance of fully-coupled implicit-explicit calculations. The mass flow within the fixture long before the thermal runaway is a result that could not be predicted by standard noncoupled calculations. In these, a thermal/chemical-coupled statics code is used to calculate the behavior until thermal runaway occurs, at which time the calculation is transferred to a hydrocode. The extrusion of energetic material cannot be predicted by such a calculation because no material motion can occur before thermal runaway. The implicit-explicit time-stepping is needed to execute fully coupled calculations. Implicit-only calculations fail at the onset of thermal runaway, and explicit-only calculations cannot handle the long heatup times. Explicit time-stepping can be made to handle long durations by variable mass scaling, where the effective time-stepping is increased during the absence of mass motion by artificially increasing the material densities; however, this approach again does not allow material motion before the onset of thermal runaway, and therefore does not accurately model the VCCT.[12] The importance of the Arbitrary Lagrangian-Eulerian (ALE) treatment is emphasized by the large material movements in this problem. The extrusion of the explosive is handled by ALE zoning, while the metal casing motion is modeled with Lagrange zoning to ensure accuracy.

## Summary of Modeling Work and Plans for Next Year

We have made major enhancements in the capabilities of ALE3D, and it now provides the tools required to model the VCCT. The implicit-explicit time-stepping allows us to track physical processes that occur on very different time scales. The ALE technique offers significant advantages in tracking the different material movements during the calculation.

Improvements remain to make ALE3D a truly predictive code. Material models for thermally degraded and/or reacting materials are needed. We need a better method for handling material models and equations-of-state for mixtures. Improved chemical reaction schemes are needed for some energetic materials. Additional data is needed in many cases to support development of these models. In addition, we plan further enhancements to the ALE3D code to provide better solution schemes, reduce calculation run times, and improve accuracy and flexibility of thermal and chemical calculations. We will address many of these in the next program year.

We also plan to incorporate a fragmenting model for the metal case, and will then calculationally study the effect of confinement on the violence of the reaction as measured by the case fracture for HMX-based energetic materials. This will allow comparison with the extensive VCCT database for these materials and will highlight further needs in code and model development.

**Timeline for Future Developments in Cookoff Violence Prediction.**

| | FY 1997 | FY 1998 | FY 1999 |
|---|---|---|---|
| Burn rate of thermally-degraded HMX. | ----------c | | |
| Improve in situ TC method. | ----------c | | |
| Measure thermal diffusivity. | ---------- | ---------- | ---------- |
| Measure burn rate of δ-HMX. | s--- | ----------c | |
| Measure burn rates at other conditions. | s--- | ---------- | ---------- |
| Try lower density samples. | | s---------- | -----c |
| Study other materials and conditions. | | | s---------- |
| Improve ALE3D code. | ---------- | ---------- | ---------- |
| Develop improved material models, reaction schemes, handling of mixtures. | s---------- | ---------- | ---------- |
| Develop fragmenting model for metal case. | s---------- | ----------c | |
| Analyze VCCT effect of confinement. | s--- | ---------- | ---------- |

## Conclusions

The Ignition and Initiation Phenomena program is aimed at the prediction of cookoff violence. We are developing the necessary analytical tool, the fully-coupled thermal/ chemical/mechanical hydrocode ALE3D, which will provide the ability to incorporate many physical and chemical processes into cookoff modeling while treating the entire cookoff problem in one calculation, as required for accurate simulation. We are also measuring key response parameters that will be incorporated into the ALE3D code, in particular burn rates and thermal diffusivities at high pressures and temperatures. Our overall goal is development of a predictive capability for the violence of thermal response of energetic materials and systems containing them, with our initial focus on HMX as a material of mutual interest to the DoD and DOE.

## Acknowledgments

We would like to acknowledge the work of Jeff Chandler, Jeff Wardell, Rich Simpson, Lonnie Daniels, and Chet Lee in support of the experimental program. We would also like to acknowledge the work of Gary L. Johnson on the VCCT modeling using ALE3D.

Finally, we thank the ALE3D development team, headed by Richard Sharp, for their efforts in support of our needs.

## References

1. W.C. Tao, M.S. Costantino and D.L. Ornellas, "Burning mechanism and regression rate of RX-35-AU and RX-35-AV as a function of HMX particle size measured by the hybrid closed bomb-strand burner," in *Proceedings of 1990 JANNAF Propulsion Systems Hazards Subcommittee Meeting*, Johns Hopkins University, Laurel, MD, Chemical Propulsion Information Agency, Laurel, MD (1990).

2. W.C. Tao, M.S. Costantino, D.L. Ornellas, L.G. Green, and E.S. Jessop, "The effects of HMX particle size and binder stiffness on the burning mechanism and regression rate of a series of fast burning propellants," Lawrence Livermore National Laboratory, Livermore, CA, UCRL-JC-104515 (June 3, 1991).

3. J.L. Maienschein, A.L.Nichols III, and C.G. Lee, *Joint DoD/DOE Munitions Technology Development Program FY-95 Progress Report*, pp. 173-192, "Ignition and Initiation Phenonema: Cookoff Violence Prediction," Lawrence Livermore National Laboratory, Livermore, CA, UCRL-ID-103482-95 (January 15, 1996).

4. J.L. Maienschein, A. Frank, A.L. Nichols, III and C.G. Lee, *Joint DoD/DOE Munitions Technology Development Program FY-94 Progress Report*, pp. 83-110, "Ignition and Initiation Phenonema," Lawrence Livermore National Laboratory, Livermore, CA, UCRL-ID-103482-94 (December 1994).

5. T.L. Boggs, "Thermal Behavior of Cyclotrimethylenetrinitramine (RDX) and Cyclotetramethylenetetranitramine (HMX)," in *Fundamentals of Solid-Propellant Combustion*, K.S. Kuo and M. Summerfield, ed., American Institute of Aeronautics and Astronautics, New York (1984).

6. R.L. Derr, T.L. Boggs, D.E. Zurn and E.J. Dibble, "The Combustion Characteristics of HMX," in *Proceedings of 11th JANNAF Combustion Meeting*, Pasadena, CA, CPIA, p. 231 (1974).

7. J. Behrens, R., "Identification of octahydro-1,3,5,6-tetranitro-1,3,5,7-tetrazocine (HMX) pyrolysis products by simultaneous thermogravimetric modulated beam mass spectrometry and time-of-flight velocity-spectra measurements," *Int. J. Chem. Kin.*, 22, 135 (1990).

8. J. Behrens, R., "Thermal decomposition of energetic materials: temporal behaviors of the rates of formation of the gaseous products from condensed-phase decomposition of octahydro-1,3,5,7-tetranitro-1,3,5,7-tetrazocine," *J. Phys. Chem.*, 94, 6706 (1990).

9. J. Behrens, R. and S. Bulusu, "Thermal decomposition of energetic materials. 2. Deuterium isotope effects and isotopic scrambling in condensed-phase decomposition of octahydro-1,3,5,7-tetranitro-1,3,5,7-tetrazocine," *J. Phys. Chem.*, 95, 5838 (1991).

10. B.M. Dobratz and P.C. Crawford, *LLNL Explosives Handbook: Properties of Chemical Explosives and Explosive Simulants*, Lawrence Livermore National Laboratory, Livermore, CA, UCRL-52997 change 2 (January 31, 1985).

11. A.L. Nichols III, "Coupled thermal/chemical/mechanical modeling of insensitive explosives in thermal environments," in *Proceedings of American Physical Society Topical Group on Shock Compression of Condensed Matter, Seattle,* American Institute of Physics Press, p. 445 (1995).

12. A.L. Nichols III, R. Couch, J.D. Maltby, R.C. McCallen, I. Otero and R. Sharp, "Coupled Thermal/Chemical/Mechanical Modeling of Energetic Materials in ALE3D," in *Proceedings of 1996 Joint Combustion and Propulsions Systems Hazards Subcommittee Meeting*, Monterey, CPIA, (1996).

13. K. Gibson, NSWC Indian Head Division, personal communication, 1995.

14. C.M. Tarver, S.K. Chidester, and A.L.Nichols III, "Critical Conditions for Impact and Shock-Induced Hot Spots in Solid Explosives," *J. Phys. Chem.*, 100, 5794 (1996).